Tropical Pacific - North Pacific teleconnection in a coupled GCM: Remote and local effects

Annalisa Cherchi[1], Simona Masina[1], and Antonio Navarra[1]

[1]Centro Euromediterraneo per i Cambiamenti Climatici, and Istituto Nazionale di Geofisica e Vulcanologia, Bologna, Italy

Manuscript submitted to

International Journal of Climatology

March 23, 2011

Corresponding author:
Annalisa Cherchi (CMCC/INGV)
Viale Aldo Moro 44
40127 Bologna, Italy
E-mail: annalisa.cherchi@bo.ingv.it
Phone: +39 051 3782613
Fax: +39 051 3782655

Abstract

The connection between Tropical Pacific and North Pacific variability is investigated in a state of the art coupled ocean-atmosphere model, comparing two twentieth century simulations at T30 and T106 atmospheric horizontal resolutions. Despite a better simulation of the frequency and the spatial distribution of the Tropical Pacific anomalies associated with the El Nino Southern Oscillation (ENSO) in the high-resolution experiment, the response in the North Pacific is scarcely different from the low-resolution experiment where the ENSO variability is weaker and at higher than observed frequency. In the North Pacific, the response of surface atmospheric fields to the variability in the Tropical Pacific appears to be affected by local coupling processes significantly different in the two experiments. The coupling between sea level pressure (SLP) and SST in the North Pacific as well as the influence of the Tropical Pacific SST has been measured here by means of the "coupled manifold" technique. In the low-resolution case the SLP variances linked to the fraction of North Pacific SST not influenced by the Tropical Pacific are weak suggesting that the remote influence is strong, consistently with the observations. On the contrary, in the high-resolution experiment the fractions and the patterns of the SLP variances due to the Tropical Pacific SST and those linked to the North Pacific SST are comparable. In the latter case, model systematic errors in the northwestern Pacific influences the local coupling processes thus triggering the remote response. We conclude that an increased atmospheric horizontal resolution does not reduce the coupled model systematic errors in the representation of the teleconnection between the North and the Tropical Pacific and that the validation of coupled models has to consider both remote and local processes.

Key words: Tropical Pacific-North Pacific teleconnection, ENSO, coupled GCMs

1 Introduction

Anomalous SST signals associated with El Niño Southern Oscillation (ENSO) occur in the Tropical Pacific, but also in other remote sites of the world ocean (Lau and Nath, 1996). Since the 70's, it was recognized that above (below) normal SST in the Equatorial Pacific were associated with cold (warm) waters in the central North Pacific (Weare et al, 1976). Searching for linear relationship between ENSO and its response in the extra tropics, the North Pacific-Tropical Pacific connection has been interpreted combining forced and local processes. In particular, tropical SST anomalies associated with ENSO force the atmospheric circulation over the North Pacific, and in turn these atmospheric anomalies produce SST changes over the extra-tropical North Pacific (Zhang et al, 1996). Heterogeneous atmospheric and oceanic processes occurring at many timescales are involved, thus increasing the complexity of the teleconnection between Tropical and North Pacific sectors (Liu and Alexander, 2007, and references therein).

Atmospheric model experiments have been widely used to demonstrate that imposed tropical SST anomalies are particularly effective in generating wave-like atmospheric response in the Northern Hemisphere during winter (e.g. Alexander, 1992; Lau and Nath, 1994; Graham et al., 1994; Ferranti et al., 1994). The extension of that kind of studies to atmospheric models coupled with mixed-layer ocean emphasized the complex nature of the role of air-sea feedback in the North Pacific response (Lau and Nath, 1996; Alexander et al., 2002), and the importance of using coupled ocean-atmosphere models to capture the impact of the ocean dynamics (Vimont et al., 2001; Liu and Yang, 2003; Yeh and Kirtman, 2008). In recent years, coupled ocean-atmosphere models have been used to perform sensitivity experiments aimed at the understanding of the explicit role of the teleconnection and of the ocean-atmosphere feedback involved (Liu et al., 2002; Wu et al., 2003; Liu and Yang, 2003; Yeh and Kirtman, 2008). Nevertheless, the identification of the portion and timescales of the extra-tropical variability modulated by ENSO or inherent to the extra-tropics is still unresolved. Current coupled models capability to simulate realistic teleconnections is a key issue, especially for implications related to the extended-range predictions of weather and climate.

In the present study, the performance of a state of the art coupled general circulation model to simulate the North Pacific-Tropical Pacific teleconnection is analyzed. A recent detailed analysis of the tropical climate variability using the same model revealed that at higher atmospheric resolution the variability in the NINO3 region (210°-270°E, 5°S-5°N) has longer time scales, involving wider latitudinal region and slower waves (Navarra et al., 2008). Building on the last result, we investigate how the improvements in the ENSO performance may impact the simulation of the

North Pacific variability and of its teleconnections with the tropics. The influence of ENSO on the North Pacific anomalies is studied in terms of composite analysis. The co-variation between SLP and SST in the North Pacific is measured by means of the coupled manifold (Navarra and Tribbia, 2005), focusing on the differences due to the atmospheric horizontal resolutions. The technique is able to separate the variance of a field into two parts, one that depends on the variability of the other field, and one that does not, obtaining a distinction between "coupled" and "free" variability (see also Cherchi et al., 2007). The coupled manifold is applied here to the SST and SLP in the North Pacific versus the SST in the Tropical Pacific. The results are then discussed in light of the differences between the model systematic errors at the two resolutions.

The study is organized as follows: section 2 describes the model, the experiments, and the datasets used for comparison with the model outputs. It contains also a brief description of the coupled manifold technique. Section 3 analyzes the model performance in simulating atmospheric teleconnection by means of an ENSO composite analysis. Section 4 investigates the North Pacific variability in winter (JFM) as co-varying with the tropics or related to local ocean-atmosphere coupling. Finally, section 5 summarizes the main conclusions.

2 Data and methodology

2.1 Model, experiments and datasets

The experiments analyzed in this study are twentieth century simulations performed with the fully coupled atmosphere-ocean general circulation model SINTEXG (Gualdi et al., 2008). The characteristics of both atmospheric and oceanic model components are described in previous publications (Cherchi et al., 2008; Gualdi et al., 2008). The same oceanic component, spatially distributed over a three-dimensional Arakawa-C-type grid (about $2^\circ \times 2^\circ$ horizontal resolution, with a meridional refinement of 0.5° at the Equator, and 31 prescribed vertical levels) has been coupled to an atmosphere with T30 and T106 horizontal truncations, corresponding to a grid of about $3.75^\circ \times 3.75^\circ$ and $1.1^\circ \times 1.1^\circ$, respectively, and 19 vertical levels.

One-member twentieth century simulations (1901-2000) at low and high atmospheric horizontal resolution (XX-T30 and XX-T106, respectively) include prescribed concentration of greenhouse gases (i.e. CO_2, CH_4 N_2O and chloro-fluoro-carbons) and sulfate aerosols, as specified for the 20C3M experiment defined for the IPCC AR4 simulations (see http://www-pcmdi.llnl.gov/ipcc/about_ipcc.php for more details).

The model outputs have been compared with observations and analysis data. In particular, the

global distribution of sea surface temperature has been taken from the HadISST dataset (Rayner et al., 2003) for the period 1901-2004, the sea level pressure and upper troposphere streamfunction fields come from the NCEP reanalysis (Kalnay et al, 1996) for the period 1948-2004, and the global precipitation is taken from the CMAP dataset (Xie and Arkin, 1997) for the period 1979-2004.

2.2 The *Coupled Manifold*

The coupled manifold is a method to analyze co-variation between fields. It is described and discussed in detail by Navarra and Tribbia (2005). In the following we report a summary of the main concepts applied to our analysis.

In the coupled manifold approach two atmospheric/oceanic fields (**Z** and **S**) are represented as data matrices. The main assumption of the statistical technique is that it is possible to find a matrix **A** representing the relationship between **Z** and **S**, and the solution is found applying the minimization problem, known as "Procrustes problem" (Richman and Vermette, 1993). In that case, the solution is expressed as:

$$\mathbf{A} = \mathbf{Z}\mathbf{S}^{'}(\mathbf{S}\mathbf{S}^{'})^{-1} \tag{1}$$

where

$$(\mathbf{S}\mathbf{S}^{'})^{-1} = \sum_{i=1}^{K} u_i \sigma_i^{-2} u_i^{'} \tag{2}$$

where u_i and σ_i are the left singular vectors and the singular values of the matrix $\mathbf{S}$, respectively, and prime means transpose. The summation extends over all its non-zero singular values. The modes that do not contribute to the variance of **S** are excluded from the inverse.

Similarly, it is possible to find an operator **B** for the problem in its "sister" form, being

$$\mathbf{B} = \mathbf{S}\mathbf{Z}^{'}(\mathbf{Z}\mathbf{Z}^{'})^{-1} \tag{3}$$

A and **B** are then two operators that express the relation between $\mathbf{Z}$ and **S**, but they are not equivalent. Applying the method described to the Empirical Orthogonal Functions (EOFs) coefficients of **Z** and **S** fields reduces significantly the mathematical dimension of the problem.

Scaling the matrices $\mathbf{Z}$ and **S** with $(\mathbf{Z}\mathbf{Z}^{'})^{-1/2}$ and $(\mathbf{S}\mathbf{S}^{'})^{-1/2}$, the new solution obtained for **A** (and **B**) contains correlation coefficients which can be checked with a significance test based, for example, on the Student distribution. When the significance test is applied to the matrix considered, the coefficients that do not fit the confidence intervals are put equal to zero, hence only

the values that are significant according to the level chosen (in our case 5%) are considered in the analysis. When considering the link between two climatic fields (say Z and S), and their reciprocal influence, it is possible to interpret the minimum between the % of variance of Z influencing S and that of S influencing Z as the "coupling" between Z and S.

The method described may identify both one-way and two-way relations between fields. In the first case we end up with "forced manifold", in the second with "coupled manifold". One of its applications is the separation between forced and free components of the variability of **Z** from the influence of the variability of **S**. In fact, using the "forced" and "free" manifold concepts (Navarra and Tribbia, 2005), **Z** and **S** may be separated as

$$\mathbf{S} = \mathbf{S}_{for} + \mathbf{S}_{free} = \mathbf{BZ} + \mathbf{S}_{free} \tag{4}$$

$$\mathbf{Z} = \mathbf{Z}_{for} + \mathbf{Z}_{free} = \mathbf{AS} + \mathbf{Z}_{free} \tag{5}$$

Hence, using for example **Z**, both $\mathbf{Z}_{for}$ and $\mathbf{Z}_{free}$ can be extracted and analyzed in terms of dominant modes of variability (EOF) or in terms of fields anomalies. An example of this application is used and described in Cherchi et al. (2007).

3 ENSO atmospheric teleconnection

ENSO is the dominant mode of variability of the Tropical Pacific sector. It is a coupled ocean-atmosphere phenomenon and it can be viewed as an oscillation from a warm to a cold phase, identified as El Niño and La Niña events (Philander, 1990). At interannual time scales, ENSO is known to influence the North Pacific variability (e.g. Alexander et al., 2002). A measure of the impact of the ENSO oscillation to the patterns of atmospheric and oceanic fields in the North Pacific sector is given in terms of composite analysis identifying warm (El Niño) and cold (La Niña) events. Here warm and cold ENSO events have been classified using the NINO3 index, following the metric described by Trenberth (1997). NINO3 index corresponds to monthly mean SSTA averaged in the Equatorial Eastern Tropical Pacific (210°-270°E, 5°S-5°N). A year is classified as a warm (cold) ENSO event if the monthly mean standard SST anomaly in the NINO3 area is larger (lower) than 1 (-1) standard deviation for at least 3 months, starting from November. A non-parametric significance test, based on the bootstrap procedure using a resampling technique (Wilks, 1995), has been applied to the composite anomalies with a significance level of 5%.

Sea surface temperature (SST) and sea level pressure (SLP) have been averaged for DJF(0/1), as ENSO peak season, and for MAM(1) as the spring season just after the peak (fig. 1). At the surface,

observed warm SST anomalies in the Equatorial Pacific Ocean are linked with cold anomalies in the northeastern Pacific Ocean (fig. 1c,f). At the Equator the maxima of the anomalies cover the equatorial Pacific from the South American coast to the middle of the basin and even farther during the ENSO peak winter. In the following season the amplitude of the anomalies decreases more in the eastern Pacific and the maxima remain localized in the centre of the basin. The negative SST anomalies in the North Pacific sector tend to reduce and to move east after the peak season (fig. 1c,f).

In XX-T30 the warm SST anomalies in the equatorial Pacific Ocean extend up to the western edge of the basin with a narrow meridional shape (fig. 1a,d). The excessive westward extension occurs even at higher resolution (fig. 1b,e) and it is associated with the cold tongue bias of the coupled model, possibly due to stronger than observed easterly equatorial winds (Guilyardi et al., 2003). On the other hand, the shape of the anomalies in terms of its meridional width improves in the XX-T106 experiment. For example, along the North American coast during both winter and spring anomalies of $\pm 0.3^{\circ}$C extend up to 35°N in XX-T106 (fig. 1b,e), while in XX-T30 they remain confined to 10°N (fig. 1a,d).

The simulated SST signature in the North Pacific is weaker than observed in both experiments. In the low resolution case it has a zonal orientation and it is localized toward the west of the basin (fig. 1a,d). Further, the intensity of the SST anomalies increases during the spring just after the ENSO peak (fig. 1d), differently from the observations (fig. 1f). In XX-T106 DJF(0/1) and MAM(1) SST anomalies in the North Pacific are drastically weaker than observed (fig. 1b,e).

The observed sea level pressure (SLP) signature in the North Pacific is evident only during the peak of the ENSO event, with large negative SLP anomalies (fig. 1c). The simulation in the coupled model is realistic in the low-resolution experiment, even if the minima are weaker than observed and they have a dominant zonal rather than meridional slope (fig. 1a). At T106 the simulated SLP anomalies have the minimum located farther north and west (fig. 1b).

A recent study using the same model but different kind of experiments revealed that a higher atmospheric resolution improves the width of the SST and upper ocean heat content anomalies in the equatorial Pacific and the temporal evolution of the ENSO events (Navarra et al., 2008). The power spectrum density of the NINO3 index (fig. 2) identifies the frequency of ENSO events as differently simulated in the low and high-resolution experiments. In XX-T30 the time series peaks at about 2 years (fig. 2, green line), while in XX-T106 the maximum is localized between 4-5 years (fig. 2, dark-red line), and it is more in agreement with the observations (fig. 2, blue line). New processes, such as the coupling of tropical instability waves and improved coastal forcing

along the South American coast, coming into play when using an atmospheric component with higher horizontal resolution, contribute to the improvements (Navarra et al., 2008).

The "atmospheric bridge", defined by Lau and Nath (1994), linking tropics and extratropics is dynamically based on the excitation of Rossby waves by tropical convection (Hoskins and Karoly, 1981), and eventually by the divergent outflow in regions of strong vorticity gradients (Sardeshmukh and Hoskins, 1988). In the observations positive precipitation anomalies computed as warm minus cold ENSO events are localized just south of the equator with a peak in correspondence of the dateline (fig. 3c). In the model the patterns simulated are different, as the maximum tends to extend through the whole basin with a quite narrow width. Moreover, opposite sign anomalies are found north of the equatorial maximum, at both resolutions (fig. 3a,b). In XX-T106 the precipitation patterns related to ENSO have positive anomalies in the western equatorial Pacific which are larger than in the low-resolution case, and positive precipitation anomalies are present also north of the Equator between the dateline and 140°W (fig. 3a,b).

The performance of the simulated precipitation anomalies in correspondence of ENSO events is influenced by the model biases in reproducing the mean winter climate. In fact, in XX-T30 and XX-T106 over the tropical band DJF mean precipitation is weaker than observed around the Equator with maximum toward the west, but stronger than observed just south of the Equator at 140°W (fig. 4a,b). In XX-T106 a further difference exists also in a narrow band just north of the equator with stronger precipitation (fig. 4b). The precipitation anomalies in XX-T106 compared to those in XX-T30 indicate that the increased atmospheric resolution is not enough to induce a real improvement in the model performance in terms of precipitation. We may speculate that a key to gain strength in the model simulation of the mean precipitation patterns and its variability related to ENSO could be to improve the parameterization of moist processes, as it has been recently shown by Zhu et al. (2009) for the Madden-Julian Oscillation (MJO).

The atmospheric response to the tropical vorticity source is seen in terms of composite anomalies of the atmospheric streamfunction in the upper troposphere (200 mb), as shown by the contours in fig. 3. In the observations a pair of anticyclones is localized in the tropical sector just east of the precipitation maximum (fig. 3c), similarly to what is expected by the atmospheric response to diabatic heating at the Equator (Gill, 1980). In the northern extra-tropics, wavelike features with centres visible in the northeastern Pacific, Canada and eastern United States (fig. 3c) characterize the flow, as discussed in the literature (Alexander et al., 2002, and references therein). In the model the origin and the wavelike propagation are less clear (fig. 3a,b). In XX-T106 a weak pair of anticyclones appears east of the precipitation maximum, that is localized too west, and the wavelike

structure in the northern extra-tropics has centres in the North Pacific, Canada and in the eastern United States coast (fig. 3b), similarly to the observations. At lower resolution the precipitation anomalies are weak and mainly localized south of the Equator extending from the western edge of the basin and beyond 140°W (fig. 3a). The anticyclones are weak and the southern one is confined in the eastern basin. In the extra-tropics, a rather zonal shape characterizes the upper tropospheric streamfunction anomalies with two main centres localized in the eastern United States coast and in the central North Pacific (fig. 3a).

In the model, the weakness of the atmospheric teleconnection in the North Pacific can be related to weaker than observed precipitation anomalies simulated in the tropical Pacific (fig. 3), as they may act as less effective vorticity sources. The computation of the Rossby wave source (RWS) in terms of upper troposphere vorticity anomalies (Sardeshmukh and Hoskins, 1988) evidences some differences in the simulation of the RWS pattern compared to the reanalysis (not shown), but the approach is not fully adequate for the identification of key differences between the model experiments and, consequently, is not enough to explain the failure of the model performance.

The mean circulation of the upper troposphere may interfere as well with the simulated atmospheric teleconnection. Fig. 4 shows the DJF mean upper tropospheric zonal wind (contours) differences between model and NCEP reanalysis. The bias at low resolution, with more intense wind in the central North Pacific (fig. 4a), may explain the tendency to have a more zonal shape of the upper tropospheric streamfunction. At higher resolution, this bias is corrected but the model tends to have more intense than observed zonal wind toward the western part of the North Pacific (fig. 4b), in correspondence of a positive bias of the precipitation pattern.

4 North Pacific variability: local coupling versus remote forcing

The differences found in the extratropical response of the SLP anomalies comparing the two experiments (fig. 1) may be related to the different simulated ocean-atmosphere local coupling. The coupled manifold technique, described in section 2.2, is used to compute the North Pacific (120°E-100°W, 20°-70°N) SLP variability linked to the SST both in Tropical Pacific (20°S-20°N) and North Pacific (20°-60°N) sectors during winter (JFM mean). All the variances computed from the coupled manifold technique for SLP and SST are summarized in Table 1.

In the North Pacific, more than one third (about 35%) of the SLP variance is associated with SST in the North Pacific (fig. 5f and Table 1) and about 23% with SST in the tropical Pacific sector (fig. 5c and Table 1), as computed in the NCEP reanalysis and HadISST datasets. In XX-T30, 37%

of SLP variance is associated with the SST in the North Pacific (fig. 5d and Table 1), and a smaller portion (29%) is linked with the Tropical Pacific (fig. 5a and Table 1). The areas of max variance in fig. 5a correspond to the regions where the North Pacific SST influences the North Pacific SLP variability (fig. 5d), suggesting that in the North Pacific the regions where the coupling is stronger are linked with the tropics. Considering North Pacific SLP and North Pacific SST, the coupling (as defined in section 2.2) is about 34% and 23% in the case of NCEP/HadISST datasets and of XX-T30 experiment, respectively (see Table 1). In XX-T106, the variance of SLP in the North Pacific linked with SST in the Tropical Pacific is comparable to the low resolution case both in terms of global quantity and of spatial distribution (fig. 5b). On the other hand, the amount of variance of North Pacific SLP linked with the SST variance in the North Pacific itself is 46%, larger than in the low resolution case but with the maxima mainly localized in the western part of the basin (fig. 5e), and the coupling is about 27% (see Table 1).

The Tropical Pacific SST can influence the link between the North Pacific SLP variability and the North Pacific SST variability because a significant fraction of the North Pacific SST variability depends on the Tropical Pacific SST variability. In fact, from the coupled manifold applied to SST in the North Pacific (120°-260°E, 20°-60°N) versus SST in the Tropical Pacific (120°-280°E, 20°S-20°N) the amount of the coupled variance is always more than one third (47%, 31% and 38% in HadISST, XX-T30 and XX-T106 experiments, respectively; see Table 1). By using the coupled manifold, the North Pacific SST is decomposed into a part that is coupled to the SST in the Tropical Pacific and a part that is independent of it. Once the North Pacific SST has been decomposed, we computed the North Pacific SLP variance linked to the component of North Pacific SST free from the influence of the Tropical Pacific SST (fig. 5g,h,i). In XX-T30 and in the reanalysis, the variances are rather weak (fig. 5g,i), confirming the idea of a weaker influence of the free North Pacific SST component on the SLP variability. On the other hand, in XX-T106 the SLP variances linked to the free SST component are as large as the values computed for the Tropical Pacific SST influence (fig. 5b and fig. 5h). Moreover, the maxima are positioned in the western part of the basin in correspondence of the regions where the influence of the North Pacific SST on the North Pacific SLP variances is larger (fig. 5e). This domain (between 40°-50°N and centered at 160°E) also corresponds to the unrealistic SST cooling associated with El Niño (fig. 1b,e), suggesting that in XX-T106 other processes are acting in response to the changes in SST and SLP. In particular, in XX-T106 the coupling between North Pacific SLP and SST variances may contribute to the misrepresentation of the surface anomalies occurring in correspondence of ENSO events.

The influence of the Tropical Pacific and North Pacific SST onto the northern extra-tropics

SLP anomalies is shown in fig. 6. Using the coupled manifold technique the dominant modes of variability of the northern extratropics (0°-360°, 20°-90°N) SLP anomalies in JFM have been computed as coupled to the Tropical Pacific SST (120°-290°E, 20°S-20°N) and to the North Pacific SST (120°-260°E, 20°-60°N). In the observations the dominant mode of variability of the SLP anomalies co-varying with the Tropical Pacific SST is characterized by a distinct pattern with centres localized in the northeastern Pacific, over Canada and in the western Atlantic/eastern United States sector (fig. 6e). A pattern similar is found when the SLP are forced from the North Pacific SST, even if the lobe over the Pacific Ocean has the max localized toward the centre of the basin (fig. 6f). However the similarities between the two panels confirm that the influence of North Pacific and Tropical Pacific SST are linked. In the model, the simulated SLP patterns are realistic when coupled to the Tropical Pacific sector at both resolutions (fig. 6a,c), but some differences are found when the coupling is computed with respect to the North Pacific SST (fig. 6b,d). In XX-T30 the SLP EOF1 coupled to the North Pacific SST is comparable to the pattern linked with the Tropical Pacific SST with the lobe over the Pacific Ocean slightly shifted toward the centre of the basin, as in the observations, and the lobe over eastern American continent/western Atlantic Ocean extending over the whole basin (fig. 6b). On the other hand in XX-T106 the SLP pattern co-varying with the North Pacific SST has a main centre localized in the North Pacific (fig. 6d), which differs from the pattern linked with the Tropical Pacific SST (fig. 6c). In XX-T106 the differences described in both fig. 5 and fig. 6 seem to be associated with the local coupling between SLP and SST in the North Pacific that interferes with the remote forcing from the tropics.

Local air-sea coupling in the extratropics may be also influenced by the simulated background state. In the North Pacific during JFM the model biases differ in the two resolutions considered. In particular, in XX-T106 the errors tend to be larger in the western North Pacific, in correspondence of the regions where the largest differences have been just discussed. In terms of SST, the model tends to have a cold bias at the Equator and warm biases within the eastern tropics close to the north and south American coasts (fig. 7). These biases are related to stronger and westward extended cold tongue simulated by the model, as previously mentioned. In the higher resolution experiment the cold biases of the tropical band are in general reduced (fig. 7b), as well as the warm biases in the eastern part of the basin. On the contrary, north of 40°N the warm bias in the northwestern Pacific (near the Japanese coast) is larger in XX-T106 than in XX-T30. In XX-T106 a cold bias (up to 1.5-2°C) is located in the whole basin north of 50°N (fig. 7b) and it may be related to the formation of the sea-ice affecting both the mean state and the variability. The steeper SST gradient north of 50°N in XX-T106 implies a winter through movement toward north and may influence

the response of the SLP anomalies to the tropical Pacific SST which in XX-T106 tend to be shifted more northward than in XX-T30.

The warm bias in the north Western Pacific is associated with an excess of latent heat flux released from the ocean to the atmosphere compared to the reanalysis (not shown), and with stronger than observed surface zonal wind stress (fig. 7, contours). In particular, in XX-T30 stronger than observed surface zonal wind stress is simulated in the 30°-40°N band extending over the whole basin (fig. 7a). At higher resolution, the bias is reduced at the center of the basin but it is larger in correspondence of the warmer SST bias in the west (fig. 7b). The intensification of the biases in the western North Pacific influences the air-sea coupling in that region, as evidenced by the coupled manifold analysis and the derived results.

To investigate the simulated SST variability in the North Pacific region an EOF analysis is performed. In the observations, the first mode of variability of the total SST field in the North Pacific has a whale shape that explains 28% of the total variance (fig. 8g), consistently with past analysis (e.g. Deser and Blackmon, 1995). When it is decomposed into a portion which variability is linked with the Tropical Pacific ("Forced" component) and a portion free ("Free" component) from that, the shapes of the first mode of variability remain similar to each other (fig. 8h,i). The spatial correlations of the "free" and "forced" components with the total SST are very high, i.e. 0.93 and 0.89, respectively. However, the comparison of the patterns shown in fig. 8 (g,h,i) suggests that when the North Pacific SST is linked with the tropical Pacific sector the maximum of the variability is located in the central-eastern part (around 160°W) of the basin between 30° and 35°N. On the other hand, when the North Pacific SST is free from the influence of the tropical Pacific the first EOF has two maxima, one in the centre of the basin (near 160°W, 35°N) and another near the Kuroshio extension at 40°N (the "whale shape" is strengthen). Actually, the distinction into different centres of action in the North Pacific dominant modes of variability has been discussed in the past, identifying that the maximum in the central North Pacific acts mainly at interannual timescale with a strong connection with the tropics, while the second one occurs at decadal and longer timescales having a weaker connection with the tropics (Deser and Blackmon, 1995; Nakamura et al., 1997). Here the application of the coupled manifold allows us to identify those features as distinct patterns in terms of connection with the tropical SST variability.

In the model experiments the "forced" and "free" patterns differ from each other both in terms of shape and explained variances (fig. 8a-f). In the total field, the first modes explain 25% and 27% of the total North Pacific SST variance for XX-T30 and XX-T106, respectively. The values are not far from the explained variance in the HadISST SST (28%), but even if the simulated first

modes of variability have a maximum toward the central eastern basin, the spatial patterns are not well correlated (fig. 8a,d). At both resolutions, the first mode of variability of the "forced" component is better spatially correlated with the total field, while the "free" component has a pattern significantly different. In particular, in XX-T30 the "forced" mode correlates with the total mode by 0.88, while the "free" one only by 0.59. Further, the shape of the first "free" mode with a max localized around 40°N and toward the western part of the basin recalls the biases in the shape of the ENSO composites, suggesting the possibility that the response of the North Pacific variability is wrongly influenced by local coupling processes simulated in the model (fig. 8c). In XX-T106, the disparity between "forced" and "free" component is even more accentuated (fig. 8e,f). In fact, the pattern correlation between "forced" and total components is very high (0.98) compared to that between "free" and total (0.39). In the high-resolution case, the free variability (fig. 8f) corresponds to a dipole between the western and eastern bounds of the North Pacific, possibly related to the simulated melting and growing of sea-ice. The differences in the "free" SST variability discussed between XX-T30 and XX-T106 is likely related to the biases described in the simulation of the mean JFM SST and zonal wind stress patterns and their influence on the simulated air-sea coupling.

Combining results from fig. 8 with previous discussions about fig. 5, the idea is that in the low resolution experiment the variability of SLP and SST in the North Pacific is strongly linked with the tropics, in agreement with the observations. On the other hand, in the high-resolution experiment the fraction of variance of North Pacific SLP coupled to the SST in the North Pacific, when free from the Tropics, is larger toward the western part of the basin (fig. 5h), in correspondence of the region where the North Pacific SST variability, free from the influence of the Tropical Pacific SST, dominates (fig. 8f). In summary, this suggests that in XX-T106 local coupling processes, possibly induced by model biases, are more active than observed, thus interfering with the tropical-extratropical teleconnection.

The time series of the North Pacific total, "free" and "forced" SST EOF1 (NPacPC1) have been regressed on the winter mean sea level pressure anomalies (fig. 8, contours) to measure the influence of the North Pacific SST variability on the atmospheric fields in the same region. In the observations, the main difference between "forced" and "free" components is that the former (fig. 8h) has larger connections toward the eastern part of the North Pacific basin (near the American coast), while in the free case the regression peaks toward the centre of the basin at 50°N (fig. 8i). In general, the pattern reproduced by the first mode corresponds to the composite anomalies previously discussed and have comparable intensities (fig. 1). In XX-T30 and XX-T106

experiments the max of the "free" North Pacific SST principal component regressed onto winter SLP anomalies is localized rather in the North (at about 55°N, fig. 8c,f). In the "forced" mode the observed tendency to have higher regression toward the eastern side of the basin is reproduced in both the experiments (fig. 8b,e) and represents the largest contribution to the total pattern.

The impact of the North Pacific variability at the global scale has been assessed by the correlation between the NPacPC1 and the global SST (fig. 9). The observed NPacPC1 is strongly correlated with SST in the tropical Pacific, Indian Ocean and Equatorial Atlantic (fig. 9g). The same pattern is maintained taking the "forced" NPacPC1 (fig. 9h), as expected. The "free" NPacPC1 remains negatively correlated with the Arabian Sea and with the tropical Atlantic Ocean (fig. 9i). In XX-T30 the total PC1 is negatively correlated with Tropical Pacific, Indian Ocean and equatorial Atlantic Ocean (fig. 9a), as in the observations even if the negative correlation with the tropical Pacific is weaker than observed (fig. 9a). The performance of XX-T106 is poor (fig. 9d-f). For example, considering the total SST, the North Pacific is not linked with the Indian Ocean and the correlation in the Tropical Pacific are confined north of the Equator and west of the dateline, even for the "forced" component.

The above result suggests that in XX-T106 the North Pacific pattern linked with the tropics is not actually linked to ENSO, or to the variability in the eastern Pacific sector, but it is associated with the patterns of the western Pacific warm pool region. For example, the regression of NINO3 index versus SST and SLP confirms that in XX-T106 the SLP pattern in the North Pacific associated with ENSO is realistic but the SST is not (not shown), in agreement with the composite shown in fig.1. The analysis performed reveals how local coupling processes likely induced by the different horizontal resolutions and model systematic errors may influence the North Pacific-Tropical Pacific teleconnection.

5 Conclusions

A comparison of two twentieth century coupled model experiments with a low (T30) and a high (T106) atmospheric horizontal resolution reveals that a better representation of ENSO does not induce, by itself, an improved connection between tropical and extra-tropical Pacific. This conclusion does not imply that a better performance of ENSO in the model is not important to simulate a more realistic connection between Tropical and North Pacific SST variations, but suggests that other processes may be active and possibly interfere negatively with it.

Equatorial SST of warm minus cold ENSO events are more realistic in high atmospheric hori-

zontal resolution experiment (XX-T106) than in low one (XX-T30), where the spatial extent of the anomalies is generally narrower and the time evolution of the event is largely faster than observed. On the other hand, in XX-T106 ENSO events have frequency peaks at about 4-5 years comparable to the observations. However, the better performance of the high atmospheric resolution experiment in terms of ENSO dynamics and frequency does not reflect into improved teleconnections between tropics and extratropics. In fact, the SST anomalies of the opposite sign in the central North Pacific and the associated SLP anomalies are poorly simulated by the model at both resolutions. This model failure can be due to a large variety of factors. In the present study we focused on the role of the mean state model biases and the coupling between sea level pressure and SST.

In the equatorial Pacific Ocean, the simulated convection in correspondence of ENSO events does not reflect the improvements described for the SST fields. In fact, in both XX-T30 and XX-T106 the precipitation anomalies are weaker than observed and extend zonally over the whole Pacific. The comparison between the two resolution results highlights some differences, but they are not enough to explain the response in the teleconnection. In the central North Pacific the higher resolution experiment improves the biases in the simulation of the mean winter upper tropospheric zonal wind, that should be important as driver of the Rossby waves coming from the tropics, but it also has a strengthening of the bias intensities in the western north Pacific, both in terms of SST and of surface zonal wind stress that trigger strong local air-sea coupling, thus influencing the remote teleconnection.

In the extra-tropics, the coupling between North Pacific SLP and North Pacific SST is measured through the coupled manifold, a powerful statistical technique that allows to analyze co-variations between climatic fields. More than one third of the variance of the sea level pressure in the North Pacific is linked with the variability of the SST in the North Pacific itself. When the SST in the North Pacific are decomposed into a part linked with the tropical Pacific SST variability and a part free from it, the coupled manifold results reveal that in XX-T30 the influence of the free North Pacific SST component is weak, suggesting that the tropics largely influence the regions where the coupling is stronger, consistently with the observations. On the other hand, in XX-T106 the SLP variances linked to the free North Pacific SST component are as large as the variances linked with the Tropical Pacific SST and they are mainly concentrated in the western part of the basin. The above results suggest that in the high resolution case in the North Pacific the coupling between SLP and SST may interfere with the response of surface anomalies to ENSO events, in agreement with the strengthening of the mean wind model biases in that region.

In summary, in the coupled model that we used a higher atmospheric horizontal resolution

does not automatically induce smaller systematic errors, at least in terms of tropical-extratropical teleconnections. In particular, a better representation of ENSO is not enough to ensure a better performance of the web of its teleconnection because other local coupling processes may interfere with them. The results of the present study are strictly model dependent, but suggest that the validation of a coupled model needs to take into account separately local and remote processes.

Acknowledgements. We thank Silvio Gualdi and Enrico Scoccimarro as they provided the high resolution model experiment. We are also grateful to the anonymous reviewers whose comments greatly improved the work.

References

Alexander MA (1992) Midlatitude atmosphere-ocean interaction during El Niño. Part I: The North Pacific Ocean. J Clim 5: 944–958

Alexander MA, Bladé I, Newman M, Lanzante JR, Lau N-C, Scott JD (2002) The atmospheric bridge: the influence of ENSO teleconnections on air-sea interaction over the global oceans. J Clim 15: 2205–2231

Cherchi A, Masina S and Navarra A (2008) Impact of extreme CO_2 levels on tropical climate: A CGCM study. Clim Dyn 31: 743–758

Cherchi A, Gualdi S, Behera S, Luo J-J, Masson S, Yamagata T, Navarra A (2007) The influence of tropical Indian Ocean SST on the Indian summer monsoon. J Clim 20: 3083–3105

Deser C, Blackmon M (1995) On the relationship between tropical and North Pacific SST variations. J Clim 8: 1677–1680

Ferranti L, Molteni F, Palmer TN (1994) Impact of localized tropical and extratropical SST anomalies in ensembles of seasonal GCM integrations. Quart J Roy Meteorol Soc 120: 1613–1645

Gill AE (1980) Some simple solutions for heat-induced tropical circulation. Quart J Roy Meteor Soc 106: 447–462

Graham NE, Barnett TP, Wilde R, Schlese U, Bengtsson L (1994) On the roles of tropical and midlatitude SSTs in forcing interannual to interdecadal variability in the winter Northern Hemisphere circulation. J Clim 7: 1416–1441

Gualdi S, E Scoccimarro and A Navarra (2008) Changes in Tropical Cyclone Activity due to Global Warming: Results from a High-Resolution Coupled General Circulation Model. J Climate 21 5204-5228

Guilyardi E, Delecluse P, Gualdi S, Navarra A (2003) Mechanisms for ENSO phase change in a coupled GCM. J Clim 16: 1141–1158

Hoskins BJ, Karoly DJ (1981) The steady linear response of a spherical atmosphere to thermal and orographic forcing. J Atmos Sci 38: 1179–1196

Kalnay E, Kanamitsu M, Kistler R, and co-authors (1996) The NCEP/NCAR 40-Year Reanalysis Project. Bull Am Meteor Soc 77 437-471

Lau N-C, Nath MJ (1996) The role of the "atmospheric bridge" in linking tropical Pacific ENSO events to extratropical SST anomalies. J Clim 9: 2036–2057

Lau N-C, Nath MJ (1994) A modeling study of the relative roles of tropical and extra-tropical SST anomalies in the variability of the global atmosphere-ocean system. J Clim 7: 1184–1207

Liu Z, Alexander M (2007) Atmospheric bridge, oceanic tunnel, and global climate teleconnections. Rev Geophys 45: RG2005 doi:10.1029/2005RG000172

Liu Z, Yang H (2003) Extratropical control of tropical climate: the atmospheric bridge and oceanic tunnel. Geophys Res Lett 30: 1230 doi:10.1029/2002GL016492

Liu Z, Shin S, Otto-Bliesner B, Kutzbach JE, Brady EC, Lee D (2002) Tropical cooling at the Last Glacial Maximum and extratropical ocean ventilation. Geophys Res Lett 29: 1409 doi:10.1029/2001GL013938

Nakamura H, Lin G, Yamagata T (1997) Decadal climate variability in the North Pacific during the recent decades. Bull Am Meteor Soc 78: 2215–2225

Navarra A, Tribbia J (2005) The coupled manifold. J Atmos Sci 62(3): 310–330

Navarra A, Gualdi S, Masina S, Behera S, Luo J-J, Masson S, Guilyardi E, Delecluse P, Yamagata T (2008) Atmospheric horizontal resolution affects tropical climate variability in coupled models. J Clim 21: 730–750

Philander GSH (1990) El Niño, La Niña and the Southern Oscillation. Academic Press

Rayner NA, Parker DE, Horton EB, Folland CK, Alexander LV, Rowell DP, Kent EC, Kaplan A (2003) Global analysis of sea surface temperature, sea ice and night marine air temperature since the late nineteenth century. J Geophys Res 18(D14) 4407 DOI:10.1029/2002JD002670

Richman MB, Vermette SJ (1993) The use of Procrastes target analysis to discriminate dominant source regions of fine sulfur in the western USA. Atmos Environ 27A: 475–481

Sardeshmukh PD, Hoskins BJ (1988) The generation of global rotational flow by steady, idealized tropical divergence. J Atmos Sci 45: 1228–1251

Trenberth KE (1997) The definition of El Niño. Bull Am Meteor Soc 78(12): 2771–2777

Uppala SM, Kallberg PW, Simmons AJ, Andrae U, da Costa Bechtold V, Fiorino M, Gibson JK, Haseler J, Hernandez A, Kelly GA, Li X, Onogi K, Saarinen S, Sokka N, Allan RP, Andersson E, Arpe K, Balmaseda MA, Beljaars ACM, van de Berg L, Bidlot J, Bormann N, Caires S, Chevallier F, Dethof A, Dragosavac M, Fisher M, Fuentes M, Hagemann S, Holm E, Hoskins BJ, Isaksen L, Janssen PAEM, Jenne R, McNally AP, Mahfouf J-F, Morcrette J-J, Rayner NA, Saunders RW, Simon P, Sterl A, Trenberth KE, Untch A, Vasiljevic D, Viterbo P, Woollen J (2005) The ERA-40 re-analysis. Quart J R Meteorol Soc 131: 2961-3012 doi:10.1256/qj.04.176

Vimont DJ, Battisti DS, Hirst AC (2001) Footprinting: A seasonal connection between the tropics and midlatitudes. Geophys Res Lett 28: 3923–3926

Weare BC, Navato A, Newell RE (1976) Empirical orthogonal function analysis of Pacific Ocean sea surface temperatures. J Phys Oceanogr 6: 671–678

Wilks DS (1995) *Statistical methods in the atmospheric sciences.* Academic Press, 467 pp.

Wu L, Liu Z, Gallimore R, Jacob R, Lee D, Zhong Y (2003) A coupled modelling study of Pacific decadal variability: the Tropical Mode and the North Pacific Mode. J Clim 16: 1101–1120

Xie P, Arkin PA (1997) Global precipitation: A 17-year monthly analysis based on gauge observations, satellite estimates, and numerical model outputs. Bull Amer Meteor Soc 78: 2539–2558

Yeh S-W, Kirtman B (2008) The low-frequency relationship of the Tropical-North Pacific sea surface temperature teleconnections. J Clim 21: 3416–3432

Zhang Y, Wallace JM, Iwasaka N (1996) Is climate variability over the North Pacific a linear response to ENSO? J Clim 9: 1468–1478

Zhu H, Hendon H, Jakob C (2009) Convection in a Parameterized and Superparameterized Model and Its Role in the Representation of the MJO. Journal of the Atmospheric Sciences 66: 2796-2811.

Tables

% of linked variances ("coupled manifold" outputs)

		NPac SLP (coupling)	NExtraTr SLP	NPac SST
NPac SST	XX-T30	37 (23)	57	
	XX-T106	46 (27)	40	
	HadISST/NCEP	35 (34)	38	
NPac SST "Free"	XX-T30	9		
	XX-T106	26		
	HadISST/NCEP	17		
TPac SST	XX-T30	29	59	31
	XX-T106	31	36	38
	HadISST/NCEP	23	44	47

Table 1. % of variance of North Pacific (NPac) SLP, North Extratropics (NExtraTr) SLP and North Pacific (NPac) SST (columns) linked with North (NPac) and Tropical Pacific (TPac) SSTs (rows) as computed from the "coupled manifold" technique (see section 4 for the description of the regions considered). "Free" is intended as the component of the SST in the North Pacific that is not influenced by the variability of the SST in the Tropical Pacific. For the link between SLP and SST in the North Pacific the coupling (as defined in section 2.2) is specified in parentheses. All the values are significant at 95%.

Figure Captions

Fig. 1. Composite of sea surface temperature (SST, shaded) and sea level pressure (SLP, contour) anomalies averaged in DJF(0/1) and MAM(1) of warm minus cold ENSO events for (a,d) XX-T30, (b,e) XX-T106 and (c,f) HadISST/NCEP datasets. Contour interval for SLP is 1 mb. SST is measured in °C. SST and SLP anomalies are masked if not significant at 95% level.

Fig. 2. Power spectrum density (PSD) of monthly NINO3 index for HadISST (blue solid line), XX-T30 (green solid line) and XX-T106 (dark-red solid line). The PSD is computed by means of the Thomson multitaper method. The dashed lines correspond to the PSD of a first-order auto-regressive model fitted on the data. For each spectrum, the peaks above the dashed line are indicative of a difference from a red-noise process.

Fig. 3. Composite of precipitation (shaded) and 200 mb streamfunction anomalies (contours) averaged in DJF(0/1) of warm minus cold ENSO events for (a) XX-T30, (b) XX-T106 and (c) XieArkin/NCEP datasets. Contour interval is $1.e^{+6}$ m^2/s, while precipitation are measured in mm/day. Precipitation and streamfunction anomalies are masked if not significant at 95% level.

Fig. 4. DJF mean precipitation (mm/day, shaded) and 200 mb zonal wind (m/s, contours) differences from Xie-Arkin and NCEP, respectively, for (a) XX-T30 and (b) XX-T106. A Student's test is applied to the differences, and they are masked if not significant at 95% level.

Fig. 5. Variance (%) of JFM North Pacific sea level pressure (SLP) associated with (a-c) JFM Tropical Pacific SST, (d-f) JFM North Pacific SST and (g-i) JFM North Pacific SST ("free" from Tropical Pacific SST influence) for XX-T30 (left), XX-T106 (middle) and NCEP/HadISST datasets (right). Contour interval is 10%. All the values shown are significant at 95%.

Fig. 6. First EOF of northern extratropics (0-360°, 20°-90°N) JFM SLP anomalies as linked with the Tropical Pacific SST (120°-290°E, 20°S-20°N) in the left panels and with the North Pacific SST (120°-260°E, 20°-60°N) in the right panels for (a,b) XX-T30, (c,d) XX-T106 and (e,f) NCEP/HadISST datasets, computed by means of the coupled manifold technique. Red solid (blue dashed) contours correspond to positive (negative) values. All the patterns shown are significant at 95%.

Fig. 7. JFM mean SST (°C, shaded) and surface zonal wind stress (N/m^2, contours) differences from

HadISST and ERA40 (Uppala et al., 2005), respectively, for (a) XX-T30 and (b) XX-T106. A Student's test is applied to the differences, and they are masked if not significant at 95% level.

Fig. 8. First EOF of North Pacific (120°E-110°W, 20°-60°N) JFM SST as total, "forced" and "free" components for XX-T30 (a,b,c), XX-T106 (d,e,f) and HadISST dataset (g,h,i). "Forced" and "free" refer to the link of North Pacific SST with the Tropical Pacific sector (120°E-90°W, 20°S-20°N), computed using the coupled manifold technique (all the values shown are significant at 95% level). The PC1 is regressed on the JFM SLP anomalies (mb) and shown as contours in each panel. A Student's test is applied to the regression coefficients to disprove the hypothesis of zero regression, and the values not significant at 95% level are masked.

Fig. 9. Correlation coefficients between total, "forced" and "free" PC1 of North Pacific (120°E-110°W, 20°-60°N) JFM SST and global JFM SST for XX-T30 (a,b,c), XX-T106 (d,e,f) and HadISST dataset (g,h,i). "Forced" and "free" refer to the link of North Pacific (120°E-110°W, 20°-60°N) SST with the Tropical Pacific sector (120°E-90°W, 20°S-20°N), computed using the coupled manifold technique. A Student's test is applied to the correlation coefficients to disprove the hypothesis of zero correlation, and the values not significant at 95% level are masked.

Figures

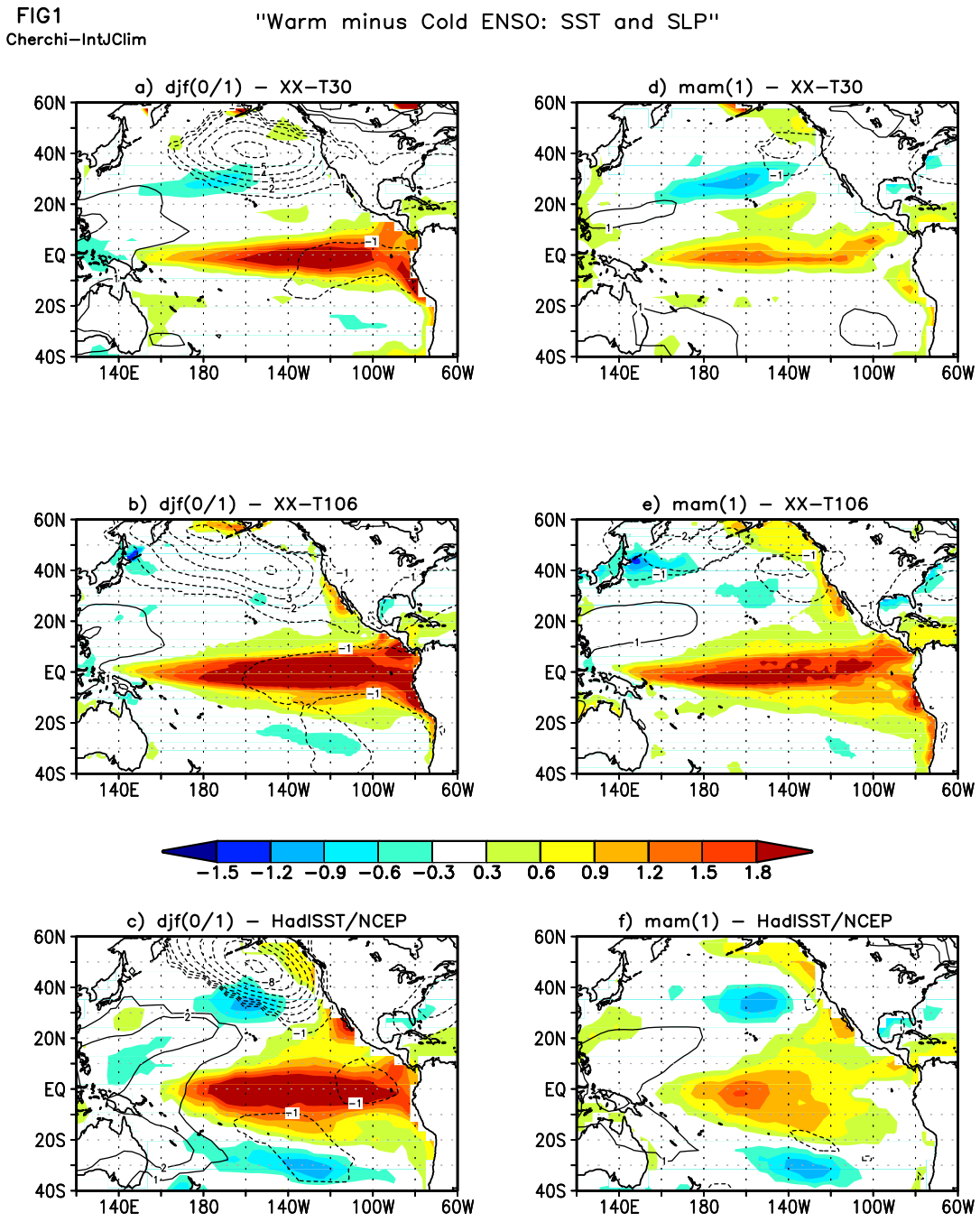

Fig. 1. Composite of sea surface temperature (SST, shaded) and sea level pressure (SLP, contour) anomalies averaged in DJF(0/1) and MAM(1) of warm minus cold ENSO events for (a,d) XX-T30, (b,e) XX-T106 and (c,f) HadISST/NCEP datasets. Contour interval for SLP is 1 mb. SST is measured in °C. SST and SLP anomalies are masked if not significant at 95% level.

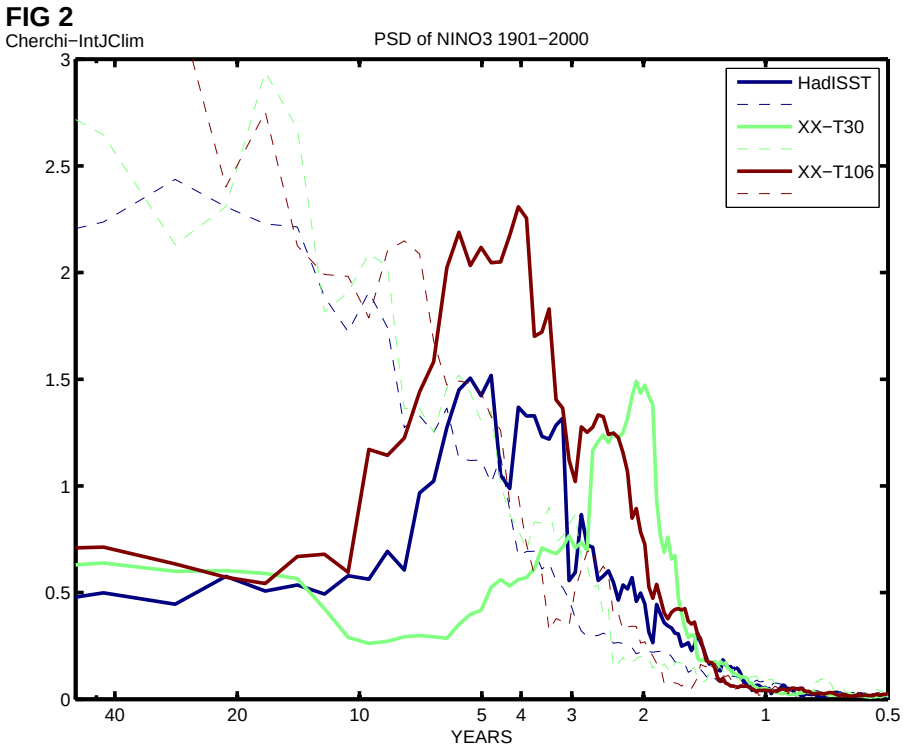

Fig. 2. Power spectrum density (PSD) of monthly NINO3 index for HadISST (blue solid line), XX-T30 (green solid line) and XX-T106 (dark-red solid line). The PSD is computed by means of the Thomson multitaper method. The dashed lines correspond to the PSD of a first-order auto-regressive model fitted on the data. For each spectrum, the peaks above the dashed line are indicative of a difference from a red-noise process.

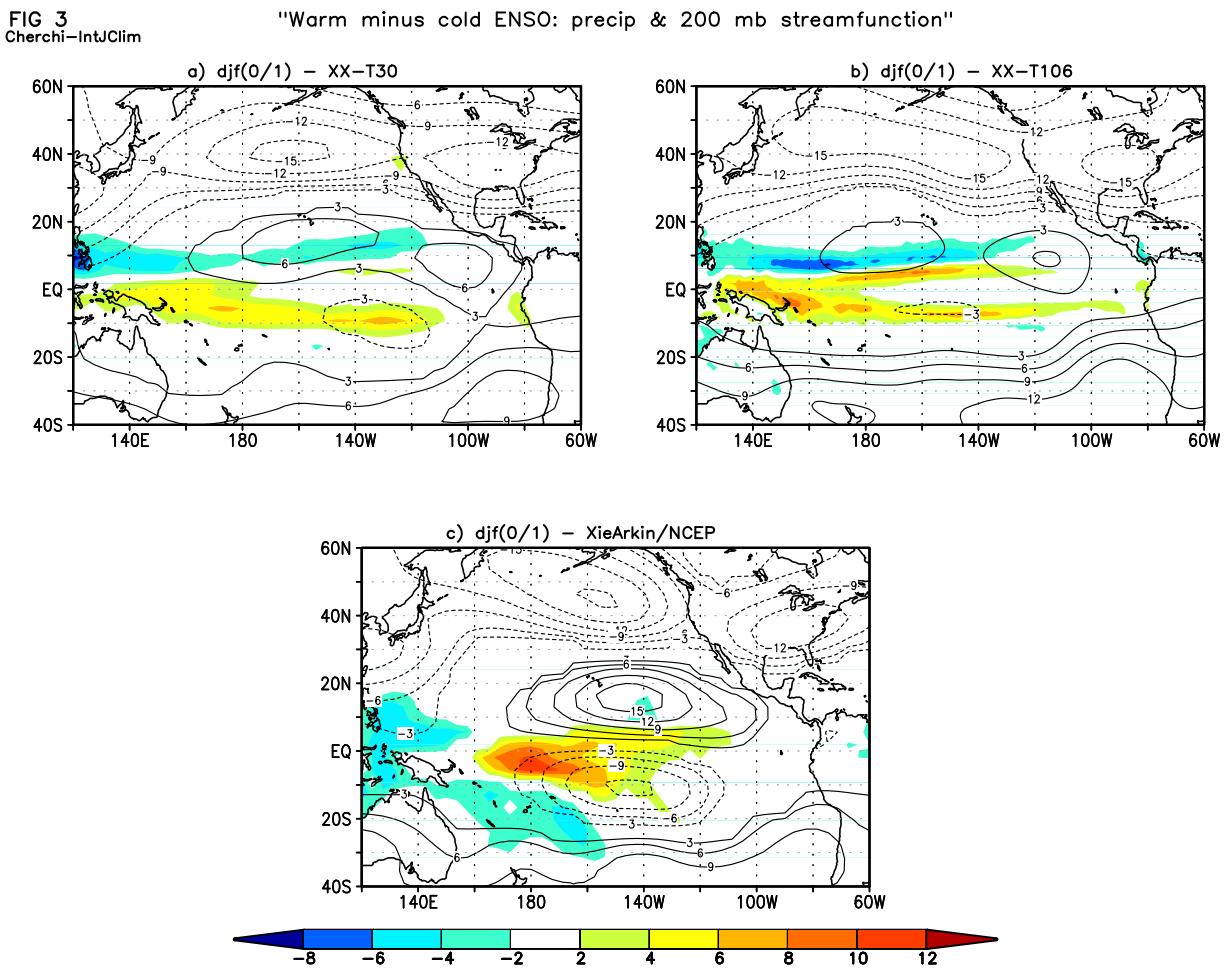

Fig. 3. Composite of precipitation (shaded) and 200 mb streamfunction anomalies (contours) averaged in DJF(0/1) of warm minus cold ENSO events for (a) XX-T30, (b) XX-T106 and (c) XieArkin/NCEP datasets. Contour interval is $1.e^{+6}$ m^2/s, while precipitation are measured in mm/day. Precipitation and streamfunction anomalies are masked if not significant at 95% level.

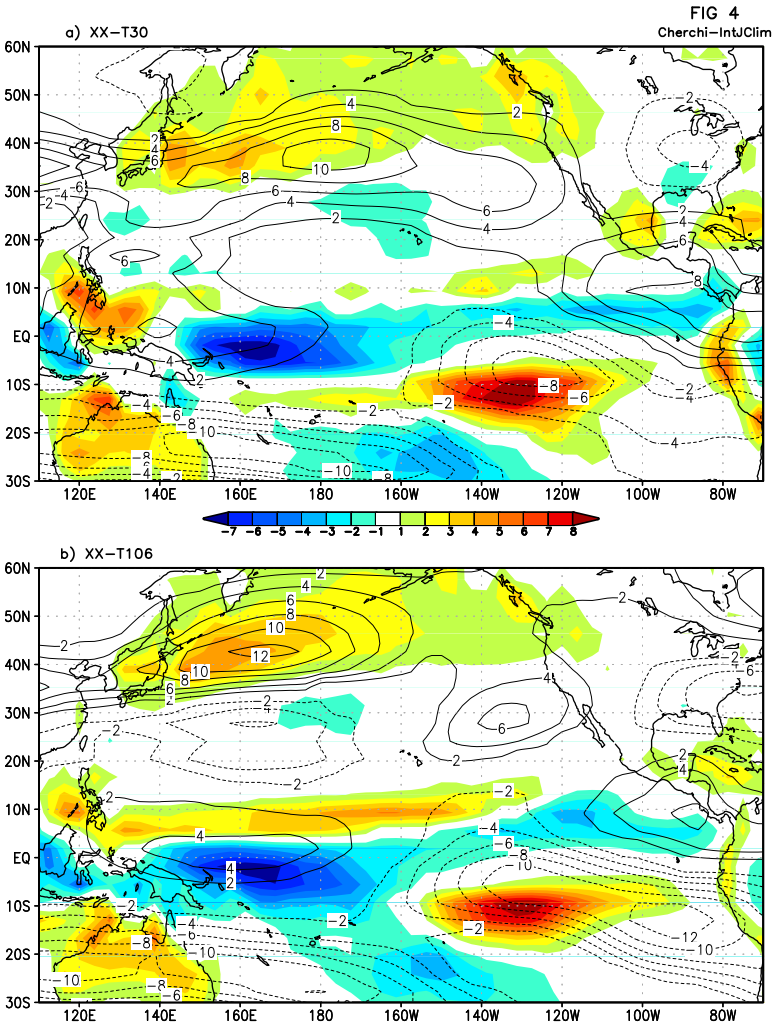

Fig. 4. DJF mean precipitation (mm/day, shaded) and 200 mb zonal wind (m/s, contours) differences from Xie-Arkin and NCEP, respectively, for (a) XX-T30 and (b) XX-T106. A Student's test is applied to the differences, and they are masked if not significant at 95% level.

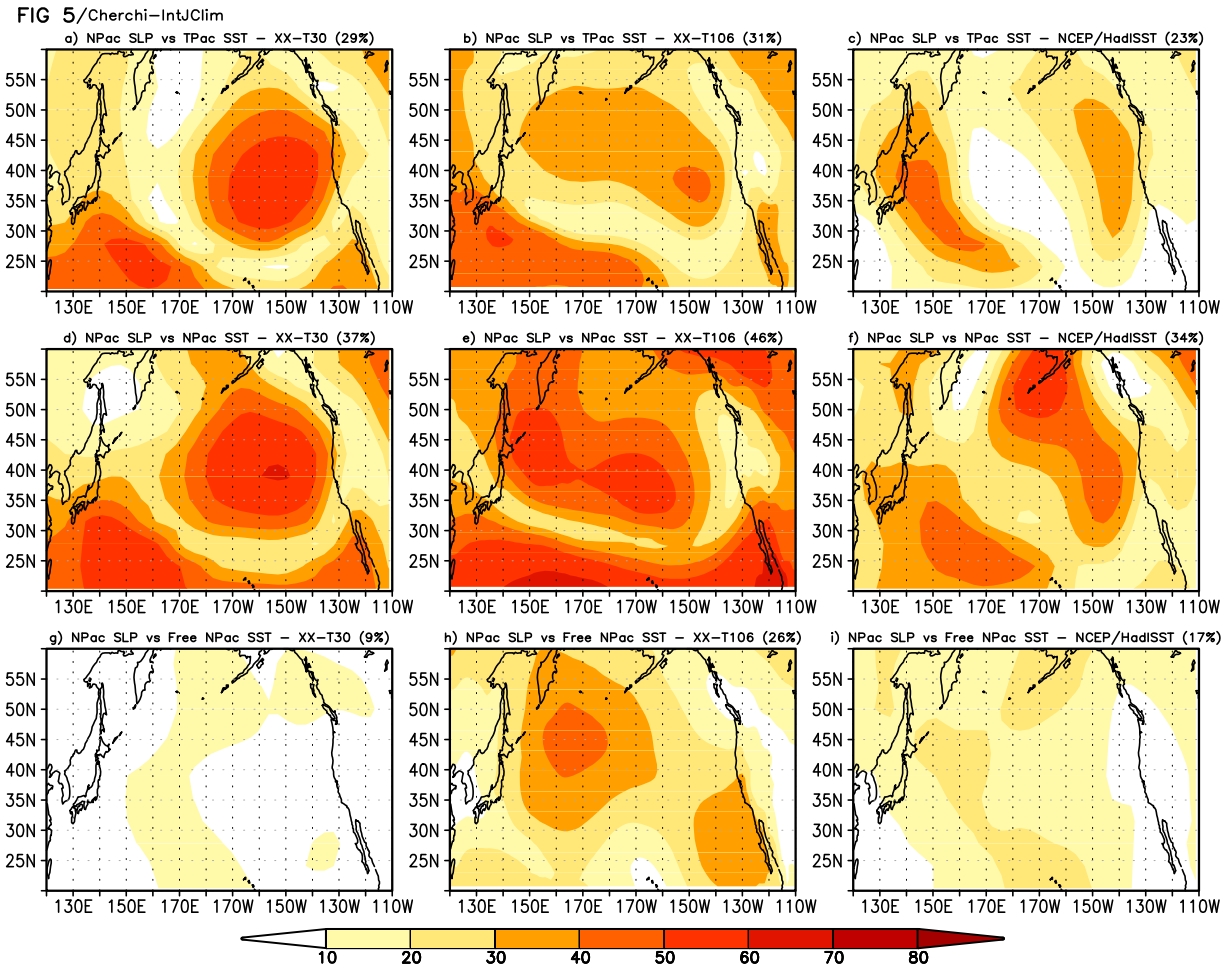

Fig. 5. Variance (%) of JFM North Pacific sea level pressure (SLP) associated with (a-c) JFM Tropical Pacific SST, (d-f) JFM North Pacific SST and (g-i) JFM North Pacific SST ("free" from Tropical Pacific SST influence) for XX-T30 (left), XX-T106 (middle) and NCEP/HadISST datasets (right). Contour interval is 10%. All the values shown are significant at 95%.

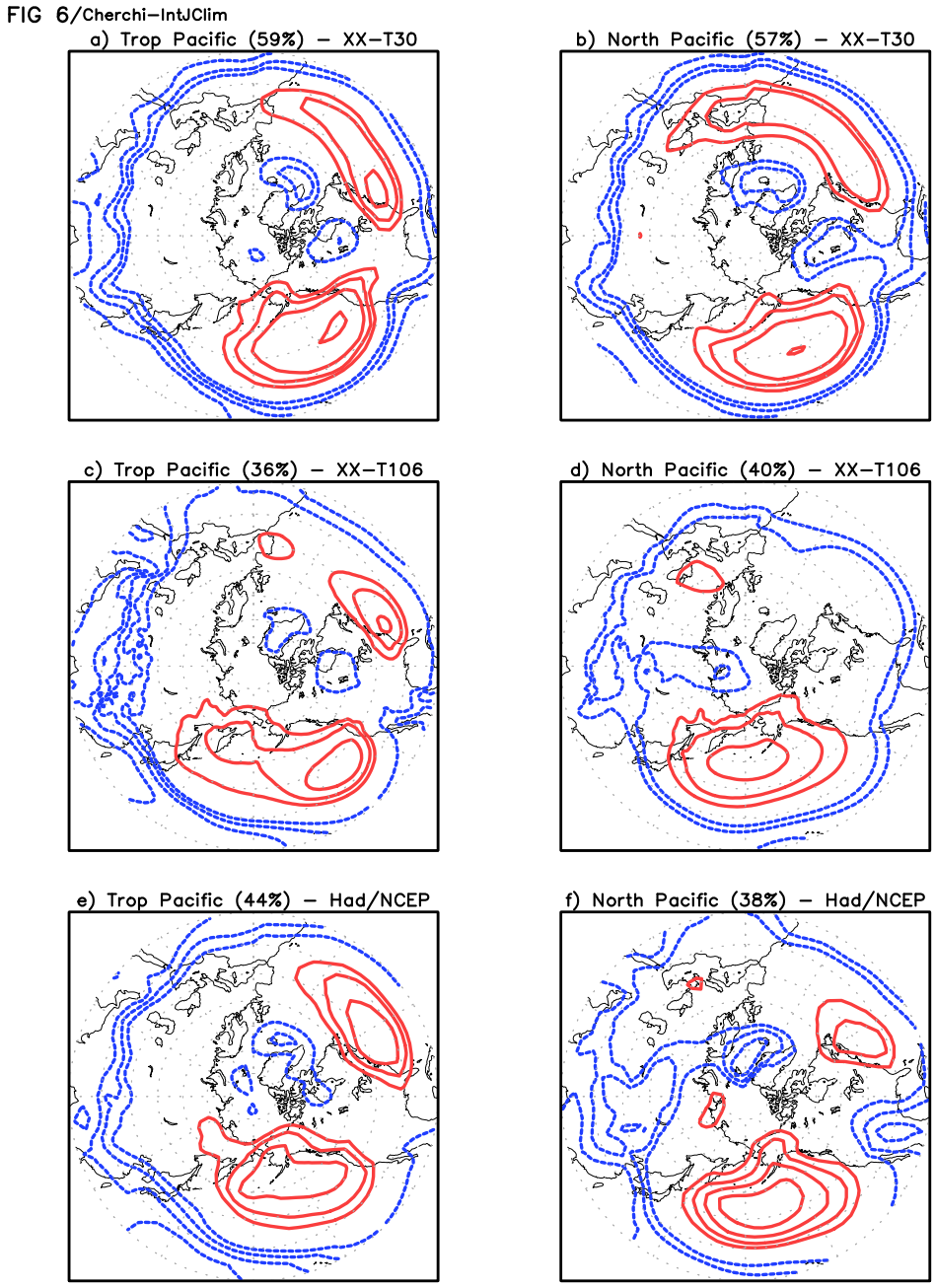

Fig. 6. First EOF of northern extratropics (0-360°, 20°-90°N) JFM SLP anomalies as linked with the Tropical Pacific SST (120°-290°E, 20°S-20°N) in the left panels and with the North Pacific SST (120°-260°E, 20°-60°N) in the right panels for (a,b) XX-T30, (c,d) XX-T106 and (e,f) NCEP/HadISST datasets, computed by means of the coupled manifold technique. Red solid (blue dashed) contours correspond to positive (negative) values. All the patterns shown are significant at 95%.

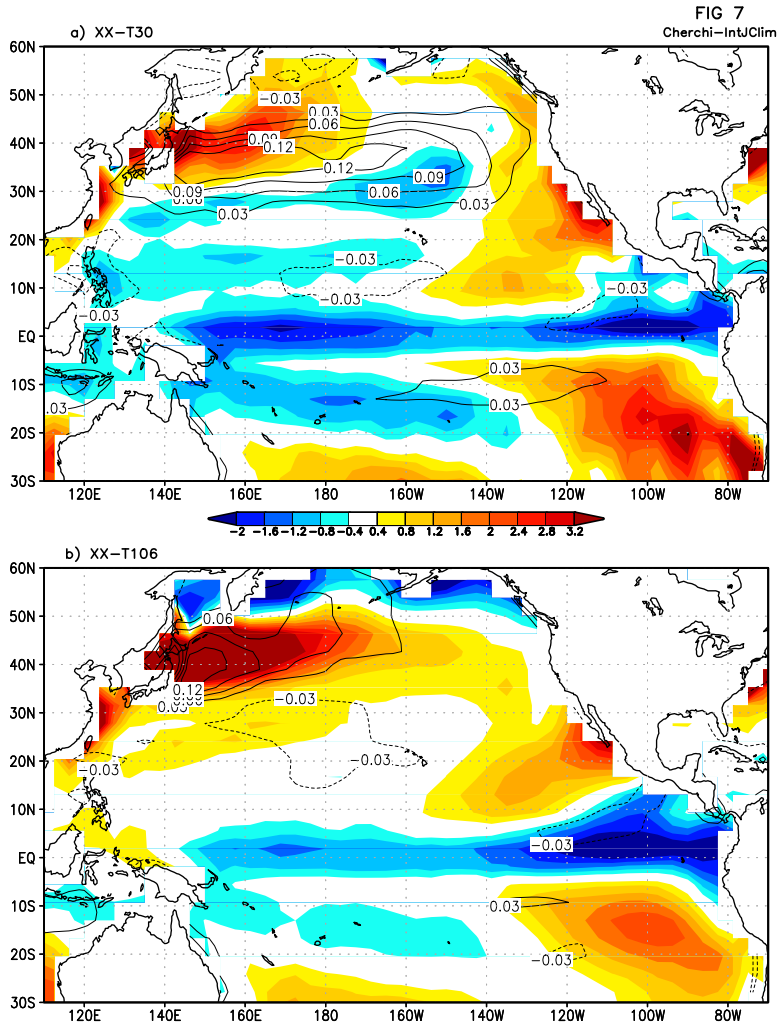

Fig. 7. JFM mean SST (°C, shaded) and surface zonal wind stress (N/m^2, contours) differences from HadISST and ERA40 (Uppala et al., 2005), respectively, for (a) XX-T30 and (b) XX-T106. A Student's test is applied to the differences, and they are masked if not significant at 95% level.

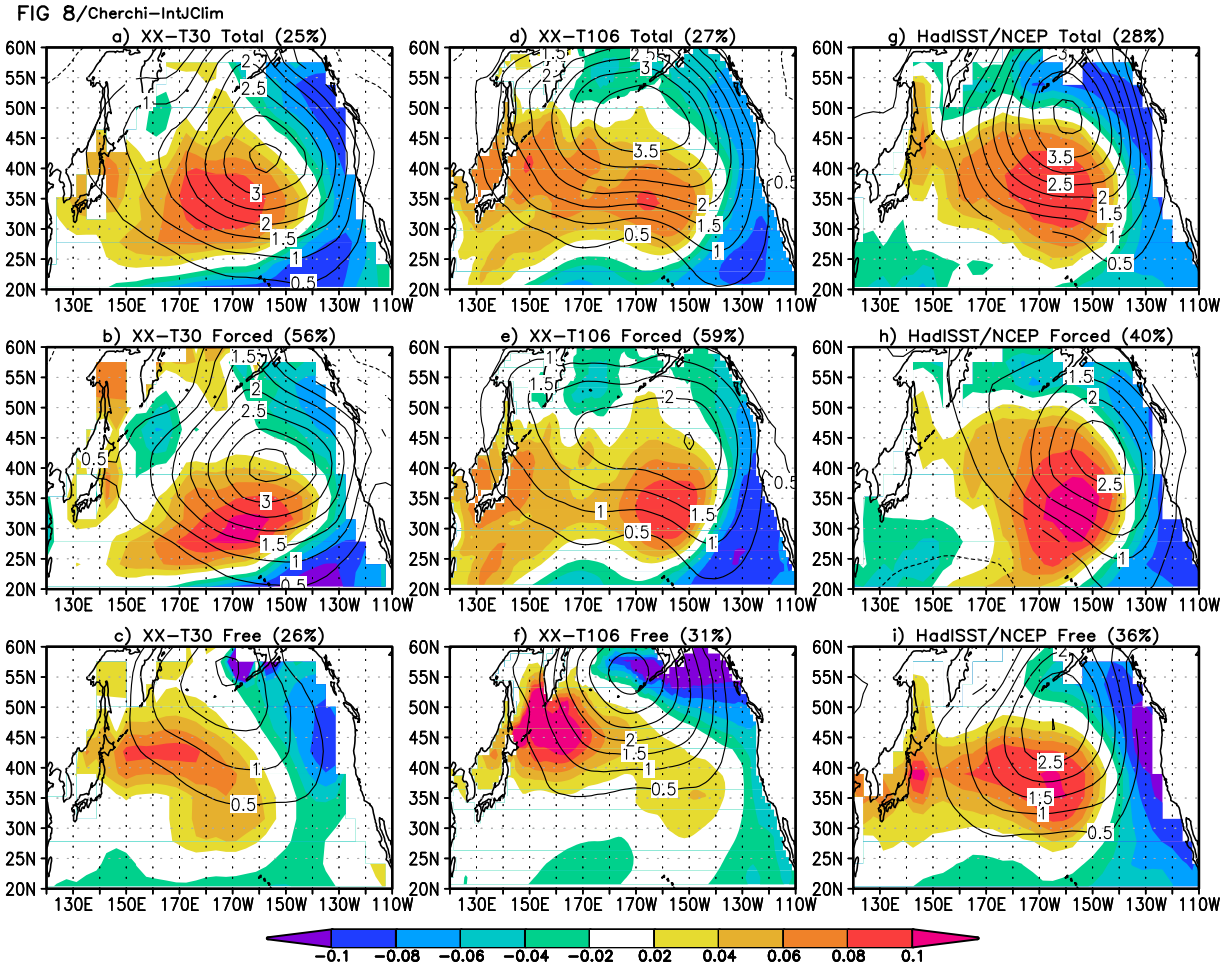

Fig. 8. First EOF of North Pacific (120°E-110°W, 20°-60°N) JFM SST as total, "forced" and "free" components for XX-T30 (a,b,c), XX-T106 (d,e,f) and HadISST dataset (g,h,i). "Forced" and "free" refer to the link of North Pacific SST with the Tropical Pacific sector (120°E-90°W, 20°S-20°N), computed using the coupled manifold technique (all the values shown are significant at 95% level). The PC1 is regressed on the JFM SLP anomalies (mb) and shown as contours in each panel. A Student's test is applied to the regression coefficients to disprove the hypothesis of zero regression, and the values not significant at 95% level are masked.

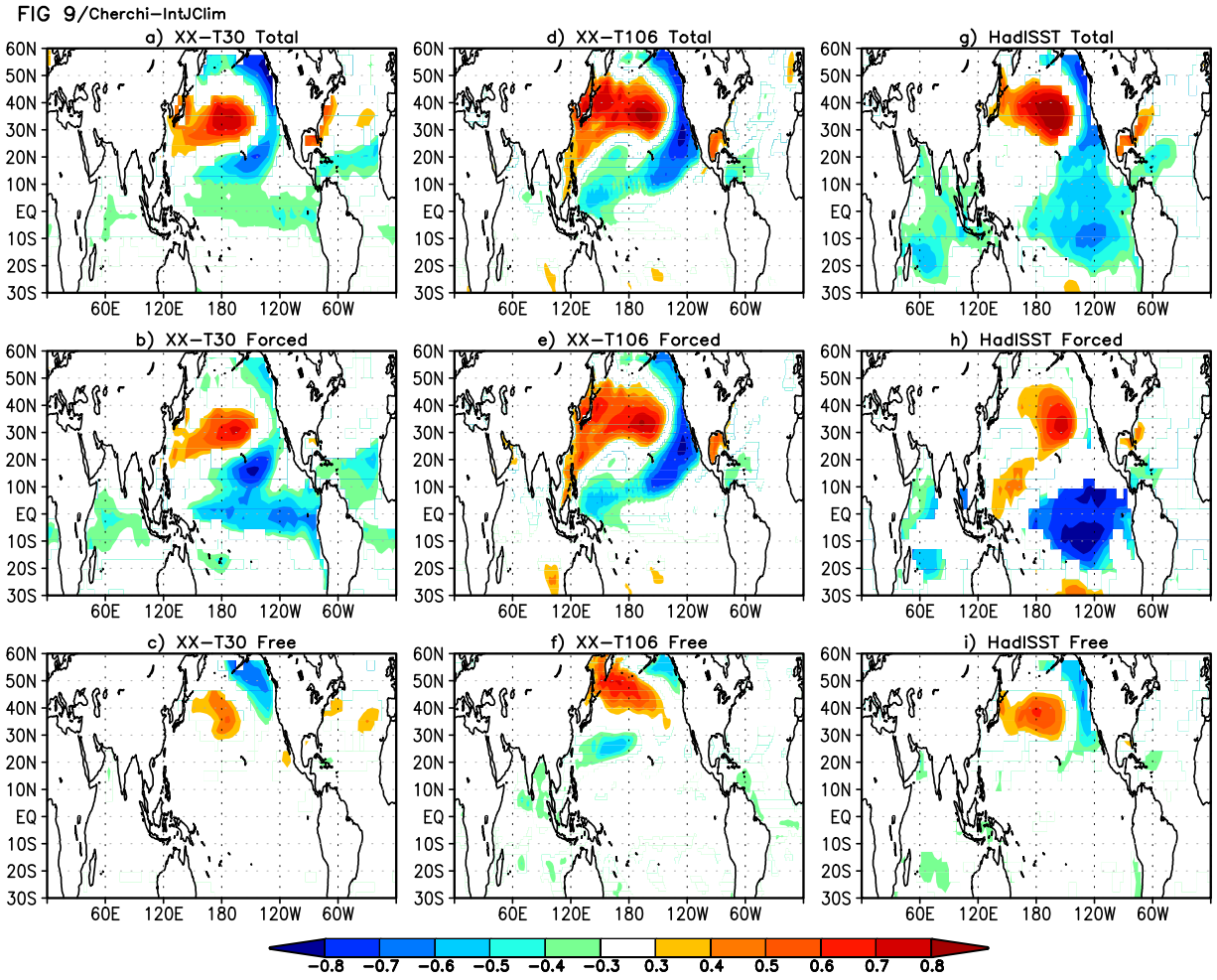

Fig. 9. Correlation coefficients between total, "forced" and "free" PC1 of North Pacific (120°E-110°W, 20°-60°N) JFM SST and global JFM SST for XX-T30 (a,b,c), XX-T106 (d,e,f) and HadISST dataset (g,h,i). "Forced" and "free" refer to the link of North Pacific (120°E-110°W, 20°-60°N) SST with the Tropical Pacific sector (120°E-90°W, 20°S-20°N), computed using the coupled manifold technique. A Student's test is applied to the correlation coefficients to disprove the hypothesis of zero correlation, and the values not significant at 95% level are masked.